New BIOTECHNOLOGY 71 (2022) 11–20

Contents lists available at ScienceDirect

New BIOTECHNOLOGY

journal homepage: www.elsevier.com/locate/nbt

Iron availability enhances the cellular energetics of aerobic *Escherichia coli* cultures while upregulating anaerobic respiratory chains

Antonino Baez [a], Ashish K. Sharma [b], Andrey Bryukhanov [c], Eric D. Anderson [d], Leba Rudack [b], Roberto Olivares-Hernández [e], David Quan [b], Joseph Shiloach [b,*]

[a] Centro de Investigaciones en Ciencias Microbiológicas, Instituto de Ciencias, Benemérita Universidad Autónoma de Puebla, Puebla 72000, Mexico
[b] Biotechnology Core Laboratory, National Institute of Diabetes and Digestive and Kidney Diseases, National Institute of Health, Bethesda, MD 20892, USA
[c] Department of Microbiology, Biological Faculty, Lomonosov Moscow State University (MSU), Moscow, Russia
[d] Mass Spectrometry Facility, National Institute of Diabetes and Digestive and Kidney Diseases, National Institute of Health, Bethesda, MD 20892, USA
[e] Departamento de Procesos y Tecnología, Universidad Autónoma Metropolitana-Cuajimalpa, Av. Vasco de Quiroga 4871, Col. Santa Fe, 05348 Mexico City, Mexico

ARTICLE INFO

Keywords:
Iron limitation
Carbon flux distribution
Chemostat
Over oxygenation

ABSTRACT

Aerobic *Escherichia coli* growth at restricted iron concentrations ($\leq 1.75 \pm 0.04$ μM) is characterized by lower biomass yield, higher acetate accumulation and higher activation of the siderophore iron-acquisition systems. Although iron homeostasis in *E. coli* has been studied intensively, previous studies focused only on understanding the regulation of the iron import systems and the iron-requiring enzymes. Here, the effect of iron availability on the energy metabolism of *E. coli* has been investigated. It was established that aerobic cultures growing under limiting iron conditions showed lower ATP yield per glucose, lower growth rate and lower TCA cycle activity and respiration, at the same time as increased glucose consumption, acetate and pyruvate accumulation, practically mimicking microaerobic growth. However, at excess iron, independent of oxygen availability, the cultures showed high cellular energetics (5.8 ATP/mol of glucose) by using pathways requiring iron-rich complex proteins found in the TCA cycle and respiratory chain. In conditions of iron excess, some iron-requiring terminal reductases of the respiratory chain, that were thought to function only under anaerobiosis, were used by the *E. coli,* when in aerobic conditions, to maintain high respiratory activity. This allowed it to produce more biomass and more reactive oxygen species that were controlled by the higher activity of the antioxidant defenses (SOD, peroxidase and catalase) and the iron-sulfur cluster repair systems.

Introduction

Iron acquisition and storage in *Escherichia coli* is controlled by the ferric-uptake regulator (Fur) which coordinates iron homeostasis in many bacteria. The expression of the *E. coli* Fur regulon is also controlled by oxygen availability [1]. Under conditions of oxygen availability and especially at over-oxygenation, the small RNA RyhB is upregulated due to Fur inactivation and, in turn, downregulates its client genes (*sodB*, *hybB*, *hybC*, *acnA*, *feoA*, and *feoB*) reducing the expression of nonessential iron-binding proteins [2–4]. However, in cultures with excess iron, over-oxygenation also activates the ferrichrome transport (FhuA) across the *E. coli* membrane [2], causing the accumulation of siderophore-iron in the cells. In aerobic growth conditions, unlike in anaerobic or microaerobic conditions, the intracellular labile Fe^{2+} pool is limited; nonetheless, *E. coli* can successfully assimilate the iron needed for its biological activity, but it is not clear how the microorganism assimilates the iron needed at elevated oxygen conditions. The purpose of this work is to understand how the bacteria overcome the potential low iron availability at over oxygenation.

Iron is an essential element for most organisms, especially for the biological activity of proteins containing iron centers, such as heme moieties, and iron-sulfur clusters. According to the EcoCyc database, *E. coli* has at least 241 genes that encode annotated iron-binding proteins, most of them involved in respiration, TCA cycle activity and DNA biosynthesis [5].

Iron exists in two predominantly redox states, the relatively soluble ferrous (Fe^{2+}) state (0.1 M at pH 7.0), which is prevalent in anaerobic conditions, and the insoluble ferric form (Fe^{3+}) (10^{-18} M at pH 7.0),

Abbreviations: Fur, ferric-uptake regulator; DMSO, dimethyl sulfoxide; TMAO, trimethylamine-N-oxide; DEG, differentially expressed gene; dO_2, dissolved oxygen.

* Corresponding author.
E-mail address: josephs@niddk.nih.gov (J. Shiloach).

https://doi.org/10.1016/j.nbt.2022.06.004
Received 5 March 2022; Received in revised form 24 June 2022; Accepted 26 June 2022
Available online 28 June 2022

which is prevalent in aerobic conditions [6]. During anaerobic growth, *E. coli* increases the intracellular labile ferrous iron (Fe^{2+}) pool by inducing the FeoABC ferrous transport system, but in aerobic conditions iron availability is limited due to the insolubility of the ferric iron. In these conditions, to cope with the low iron availability, *E. coli* activates the expression of the Fe^{3+} uptake systems (enterobactin and ferrichrome), to increase iron uptake [1].

Aerobic iron metabolism in *E. coli* K-12 has been studied under iron-limiting conditions where iron availability was limited by the addition of the iron chelator 2,2'-dipyridyl (dip) at 200 mM, which triggered the expression of several iron-acquisition genes. Among them are those involved in Fe-enterobactin transport, Fe-hydroxamate transport, enterobactin biosynthesis, Fe-S formation, Fe-siderophore transport, and Fe-citrate transport [7]. At these conditions, genes encoding for cytochromes, nitrate reductase, and the fumarate reductase complex were downregulated. The dip chelator also induces the small RNA RyhB, repressing the synthesis of many iron-binding proteins, which increases intracellular levels of iron [8].

Iron-limited cultures of *E. coli* MG1655 under aerobic conditions at nonlimited glucose are characterized by lower biomass yield and higher acetate accumulation compared with glucose-limited cultures [9]. Proteomic analysis has shown that the abundance of glyceraldehyde-3-phosphate dehydrogenase, phosphoglycerate kinase, enolase and pyruvate kinase increased at low iron conditions; all these enzymes are involved in the energy generation phase of glycolysis. It is, therefore, not surprising that at these iron-limited conditions, the abundance of iron-dependent enzymes of the TCA cycle was decreased [10,11].

Although iron homeostasis has been studied in *E. coli* batch and continuous cultures [4,7,10], most of these studies were focused on understanding the regulation of iron import systems and iron-requiring enzymes. The purpose of this work is to determine how iron availability affects the energy metabolism of *E. coli* without the toxic effect of iron chelators. Low iron availability in aerobic cultures decreased growth yield and respiration while increasing glucose consumption, accumulation of pyruvate and acetate, mimicking microaerobic conditions. Iron-limited cultures showed lower respiration rates caused mainly by the low expression of NADH dehydrogenase I, hydrogenase 2, and downregulation of nitrate, dimethyl sulfoxide (DMSO), trimethylamine-N-oxide (TMAO), and fumarate reductases terminals. Finally, a global metabolic analysis for aerobic iron-limited cultures is presented in terms of cellular energetics.

Materials and methods

Bacterial strains, inoculum preparation and culture media

E. coli MG1655 (F-, λ, ilvG-, rfb-50, rph-1) was grown at steady-state conditions in a defined medium with the following composition: KH_2PO_4, 13 g/L; $(NH_4)_2HPO_4$, 4 g/L; citric acid, 1.5 g/L. The pH was adjusted to 7.0 with 5 M NaOH prior to sterilization, and after sterilization the medium was aseptically supplemented with 1 mL/L of trace metal solution with or without 100 μM iron [12], 5 mM $MgSO_4$, 4.5 mg/L thiamine-HCl, and 8 g/L glucose. Frozen stocks were used to inoculate overnight precultures grown at 37 °C in 100 mL of defined medium with 5 g/L of glucose. All chemicals were purchased from Sigma-Aldrich (St. Louis, MO, USA).

Bioreactor culture conditions

Continuous cultures were performed in triplicate at a dilution rate of 0.4 h^{-1} in a 5 L bioreactor (Sartorius, Göttingen, Germany) with and without iron limitation. The temperature was maintained at 37 °C and pH was controlled at 7 by NH_4OH (25 %) addition. Dissolved oxygen (dO_2) concentration was measured with a polarographic oxygen electrode (Mettler Toledo, Columbus, OH, USA) and was controlled at 6.3 %, 21 %, 42 %, and 63 % of pure oxygen saturation. Two-point calibration of the dissolved oxygen electrode was performed by bubbling nitrogen for zero and pure oxygen for 100 % saturated. After calibration, regular air was bubbled into the bioreactor to confirm a dO_2 value of 21 %. The working volume of the cultures was kept at 2 L by two peristaltic pumps, one for effluent and the other for feeding sterile medium. Continuous cultures were initiated with a dO_2 set value of 6.3 % (equivalent to 30 % air saturation), and after five residence times, when a steady state was confirmed, fermentation samples were taken for dry weight, metabolites, RNA and protein isolation. At this point the dO_2 was increased to 21 % (equivalent to 100 % air saturation), followed by an increase to 42 % (equivalent to 200 % air saturation) and 63 % (equivalent to 300 % air saturation), by using a pure oxygen-air mixture as inlet gas. Samples for glucose and acetic acid assays were centrifuged and immediately filtered (0.2 μm pore size filter, Millipore) and kept at − 20 °C until analysis. Samples for proteomic analysis were centrifuged at 20,800 × *g* for 5 min at 4 °C, washed with phosphate buffered saline (PBS), and the pellets quickly frozen in a dry ice-ethanol mixture and stored at − 80 °C. For RNA-seq, 1 mL of fermentation samples were added to 4 mL RNAprotect reagent (Qiagen, Valencia, CA, USA), mixed, and incubated for 5 min at room temperature. After centrifugation for 10 min at 5000 × *g*, the supernatant was discarded and the pellets were suspended in 1 mL TRIzol reagent (Life Technologies, Carlsbad, CA, USA), frozen immediately in dry ice and stored at − 80 °C. Off gas (oxygen and carbon dioxide) composition was analyzed online by using a BlueInOne Ferm (BlueSens, Herten, Germany) gas analyzer. Online respiration activity was calculated from O_2 and CO_2 transfer rates, which were calculated performing oxygen and CO_2 mass balance between the inlet and outlet gas composition data, as specified in the following equations.

$$OTR = \frac{P}{RT_i} * \frac{F_i}{V_L} * \left(Y_{O2,i} - R_i * Y_{O2,o}\right)$$

$$CTR = \frac{P}{RT_i} * \frac{F_i}{V_L} * \left(R_i * Y_{CO2,o} - Y_{CO2,i}\right)$$

$$R_i = \frac{1 - Y_{O2,i} - Y_{CO2,i} - Y_{H2O,\ \ i}}{1 - Y_{O2,o} - Y_{CO2,o} - Y_{H2O,o}}$$

Where OTR is the oxygen transfer rate (mole L^{-1} min^{-1}); CTR is the carbon dioxide transfer rate (mole L^{-1} min^{-1}); P is the absolute pressure of gaseous stream (atm), R is the ideal gas constant (L atm mol^{-1} K^{-1}), T is the temperature of gaseous stream (K), F is the gas flow rate (L min^{-1}), V_L is the reactor working volume (L), R_i is the inert ratio, y_{O2} is the oxygen molar fraction, y_{CO2} is the carbon dioxide molar fraction, i and o subscripts denotes the inlet and outlet, respectively.

Analytical methods

Cell growth was followed by measuring culture Optical Density (OD) at 600 nm (Ultrospec 3000 UV/Visible spectrophotometer, Pharmacia Biotec, PA, USA); the measurement values were converted to dry cell weight (DCW) per liter using a calibration curve (1 OD600 nm = 0.403 gDCW/L).

Glucose and lactate concentrations were determined by YSI 2700 Biochemistry Analyzer (YSI Instruments, Yellow Springs, OH, USA). The acetic acid concentration was determined using the R-Biopharm AG (Darmstadt, Germany) Kit (Cat. No. 10 148 261 035). Siderophore concentration was measured by using the chrome azurol S (CAS) competitive iron-binding capacity assay [13].

Pyruvate, glutamate, and hypoxanthine concentrations were determined by using the Rigol L-3000 HPLC system (Rigol Technologies, Inc. Beijing, China). Chromatographic separation was performed on a Kromasil C18 column (250 mm × 4.6 mm, 5 μm) (Sigma-Aldrich, St. Louis, MO, USA) with column temperature set at 30 °C for pyruvate and hypoxanthine, and 40 °C for glutamate. The mobile phase for pyruvate consisted of two solutions, solution A (182.6 mg K_2HPO_4 and 1415 mg

KH_2PO_4 dissolved in 800 mL ultrapure water) and solution B (200 mL methanol) with isocratic elution 40 min. The detection wavelength was 325 nm. The flow rate was 1.0 mL/min and the injection volume was 10 µL. The mobile phase for hypoxanthine was 5 mM KH_2PO_4, with isocratic elution for 40 min. The UV detection wavelength was 254 nm. The flow rate was set at 1.0 mL/min and the injection volume was 10 µL. The mobile phase for glutamate consisted of two effluents: solution A (7.6 g CH_3COONa dissolved in 70 mL acetonitrile and 925 mL ultrapure water) and solution B (80% acetonitrile, 20 % H_2O). The following gradient was used: 100 % solution A for 2 min, 0–45 % solution B for 31 min, 100 % solution B for 5 min, and then equilibration at 100 % solution A for 7 min to restore the initial condition. The flow rate was set at 1.0 mL/min and the injection volume was 10 µL. For pyruvate sample preparation, culture supernatants (0.2 mL) were extracted with 0.2 mL extraction reagent (5 mg EDTA dissolved in 76 mL ultrapure water and 4 mL of HCl solution 4 M) and mixed with 0.3 mL ultrapure water and stored at − 4 °C for 60 min. Precipitates were removed by centrifugation at 17,000 *g* and 4 °C for 10 min. Supernatants (0.25 mL) were alkalinized by the addition of 50 µL NaOH 0.2 M and derivatized with 200 µL phenylhydrazine hydrochloride (55 mM) in 175 µL of PBS, pH 7.4 120 mM, for 30 min at 25 °C. For hypoxanthine sample preparation, 0.5 mL culture supernatants were hydrolyzed with 1 mL $HClO_4$ at 100 °C for 60 min followed by NaOH addition to adjust the pH to 3.8, the resulting solution was dried and reconstituted with 1 mL NaOH for HPLC analysis. For glutamate sample preparation, culture supernatant (0.2 mL) was mixed with 0.2 mL amino acid standard solution, added with 20 µL norleucine for the internal standard, 100 µL (C2H5)3N-acetonitrile and 100 µL phenyl isothiocyanate acetonitrile, vortexed, kept at 25 °C for 60 min. Thereafter, 400 µL hexane was added to each extract, vortexed, and centrifuged. The lower layer was collected and filtered through a 0.22 µm membrane for HPLC analysis.

Enzyme activities

To measure the activities of the antioxidant enzymes, 50 mL culture was centrifuged at 9000 × *g*, 4 °C, for 20 min, and the cell pellet was suspended in 5 mL of ice-cold potassium phosphate buffer 50 mM, pH 7.8. Cells were disrupted by sonication, using an Ultrasonic Homogenizer Processor XL (Cole-Parmer, IL, USA) (15 s with 45 s short-term cooling in ice, 12 series), the cell debris was removed by centrifugation for 20 min at 20,000 *g* and 4 °C, the supernatant was stored in aliquots at − 20 °C until use, and the protein concentration was measured by Pierce BCA Protein Assay Kit (Cat. No. 23225 Thermo Fisher Scientific, IL, USA). The catalase activity in the cell-free extracts was determined spectrophotometrically (1 cm cuvette, PharmaSpec UV-1700 spectrophotometer) at 240 nm. The catalase enzyme-mediated dismutation of hydrogen peroxide into molecular oxygen and water was followed as a change in absorbance at 240 nm in 50 mM potassium phosphate buffer, pH 7.0 with $\varepsilon_{240} = 39.4\ M^{-1}\ cm^{-1}$ [14]. One unit of catalase decomposes 1.0 µmole of H_2O_2 per 1 min at pH 7.0 and 25 °C, when 10.3 mM initial concentration of H_2O_2 is used. The peroxidase activity was determined spectrophotometrically using 2,2'-azino-bis-3-ethylbenzthiazoline-6-sulfonic acid (ABTS) as a substrate [15]. The assay mixture in deionized water (1 mL of reaction volume) contained 96 mM potassium phosphate (pH 5.0), 8.7 mM ABTS, 0.01 % (w/w) H_2O_2, 0.004 % (w/v) bovine serum albumin and 0.008 % (v/v) Triton X-100. One unit of peroxidase oxidizes 1.0 µmole of ABTS per 1 min at pH 5.0 and 25 °C, $\varepsilon_{405} = 36.8\ M^{-1}\ cm^{-1}$. The rate of accumulation of oxidized ABTS was followed by the increase in absorbance at 405 nm. Superoxide dismutase (SOD) activity was determined spectrophotometrically at 550 nm by the xanthine oxidase-cytochrome *c* method [15]. The assay mixture in deionized water contained 50 mM potassium phosphate (pH 7.8), 0.1 mM EDTA, 50 µM xanthine, 10 µM cytochrome *c*, and 5 mU xanthine oxidase. One unit of SOD inhibits the rate of reduction of cytochrome *c* by 50 % in a coupled system, using xanthine and xanthine oxidase as an enzymatic source of the superoxide radical at pH 7.8 and 25 °C.

Total RNA isolation and RNA-seq analysis

Total RNA was isolated from the frozen cells in Trizol samples collected from three independent runs from iron-restricted and iron-available cultures using the hot phenol method [16]. The ribosomal RNA was depleted from the purified total RNA by using the RiboMinus Transcriptome Isolation Kit (Invitrogen, Carlsbad, CA, USA), following the manufacturer's instructions. RNA concentration and quality were assayed using NanoDrop 2000 Spectrophotometer and Bioanalyzer 2100 (Agilent Technologies, Sta. Clara, CA, USA). The RNA-seq libraries were prepared using the TruSeq Stranded Total RNA with Ribo-Zero Plus (Illumina, San Diego, CA, USA) for Illumina as described in [16]. Initial cDNA library was quantitated using PicoGreen assay. The cDNA library samples were sequenced in Illumina Novaseq6000 for the complete transcriptome sequencing. The RNA-seq data processing was done as described in [16]. dO_2 point samples were processed using biological triplicates from three different continuous culture runs. ANOVA was performed to compare transcriptome profiles among cultures at unrestricted and restricted iron conditions. Significant differentially expressed genes (DEGs) were obtained by using filtering criteria of *p*-value and fold change cut off of less than or equal to 0.05 and 1.50, respectively. Pathway enrichment analysis and regulatory interactions on the DEGs was done using the Partek genomics suite and omics dashboard tool of EcoCyc [17], respectively.

Proteomics analysis

Frozen pellet samples were resuspended in 1 % sodium dodecanoate [18], heated to 90 °C for 10 min, then bacterial cells were disrupted in a Diagenode bioruptor (Denville, NJ, USA) using three 10-min cycles at setting 3 at 50 % duty cycle without concern for heating (but the bath stayed below 32 °C). Bacterial extracts were reduced, alkylated, digested with trypsin, and freed of soap through acidification and three ethyl acetate extractions as described by [18] except that chloroacetamide was used in place of iodoacetamide [19]. One-third of the volume obtained from each sample were pooled to serve as an internal standard. The pool and the remaining sample were loaded (separately) on C8/C18 Stage tips (the pool distributed over two column sets) and subjected to on-column reductive dimethylation with each sample receiving either an "M" or "H" chemistry labeling reaction following protocol C in [20] and the "pool" sample received the "L" chemistry. As detailed in the reference [20] "L" peptides have two normal methyl groups, "M" peptides have two methyl groups each with two deuterons, and "H" peptides have three deuterons and a carbon-13 making up each of the two methyl groups on each original amino group. After elution, the same portion of the pool eluate ("L") was added to each pair of sample eluates made up of an "M" and "H" reacted sample, and these carefully "doped" samples were dried under nitrogen and resuspended in 30 µL 0.1 % formic acid 2 % acetonitrile and analyzed essentially as described by [21] but with a Thermo nLC-1000 (operating at 0.1 µL/min for separation) and a single column configuration 500 cm Easy Spray column (Thermo Fisher Scientific, IL, USA) in place of the NanoAcquity two column configuration. Because only higher abundance proteins were of interest, prefractionation was not needed.

The "L" pool sample is made up of an equal contribution of each of the samples being analyzed and the same amount is used in each combination ("L" + "M" + "H") where the "M" and "H" channels are occupied by the original samples in a series of runs. Using MaxQuant (21) a median estimate based on all observations from a particular protein group of the M/L or H/L ratios are obtained. Because the make-up of the material in the L channel is the same, these ratios provide an estimate of the relative amount of protein in each of the samples used to make up the "M" and "H" channels, being normalized to the abundance of the protein present in the "L" sample. Because the same pool type standard

was used for each sample, the tables resulting from analysis display the program's best estimate of protein abundance for each sample in a proportional way with each protein on its own scale, i.e. values were normalized per protein to generate quantitative ratios. To generate metabolic maps, readings from the same condition were averaged, comparisons between conditions were made as ratios of these average ratios, and the resulting values were normalized to zero via a natural log transformation. These log transformed values were superimposed onto a cellular overview of metabolism for E. coli K-12 substrain MG1655 available on ecocyc.org.

Flux distribution calculations

The genome-scale metabolic model iJO1366 of *E. coli* was used to explore the metabolic fluxes [22]. Flux balance analysis (FBA) is a method that uses linear programming to calculate the flux distribution [23,24]. The consumption rates of glucose, O_2, and CO_2, and the production rates of acetate, glutamate, hypoxanthine and pyruvate were used as constraints to predict the growth rate as the objective function for either iron-limited or iron-excess conditions. The flux distribution was calculated using the COBRA Toolbox in Matlab 2020 [25].

Statistical analysis

The statistical analysis of kinetic parameters, metabolite concentrations, and enzyme activities values was performed using Sigma Plot (Systat Software Inc., Palo Alto, CA, USA). Data were analyzed globally by analysis of variance (ANOVA) single factor, and significant treatment effects were determined by Fisher's LSD test. Bioassays were performed three times with three replicates per treatment.

Results

Effect of dissolved oxygen on biomass production, glucose consumption, and acetate excretion in E. coli growing at steady state with and without iron limitation

To determine how iron availability alters the energy metabolism of *E. coli* K-12 (MG1655 strain), iron-limiting cultures were performed under steady-state conditions with different oxygen concentrations (Supplementary Fig. 1). By using this approach, any changes in the cellular energetics would be the result of iron availability and not of growth rate or growth phase. The bacteria were grown in a minimal medium with and without 100 μM $FeCl_3$ supplementation. The concentration of the contaminating iron in the medium without iron addition was 1.75 ± 0.04 μM, making the ratio of ferric iron (Fe^{3+}) to ferrous iron (Fe^{2+}) 1.12, while the total amount of iron in the culture with iron supplementation was 105.56 ± 0.23 μM, making the ratio of ferric iron (Fe^{3+}) to ferrous iron (Fe^{2+}) 19.7. Independent of the dO_2 concentration, steady-state cultures with iron limitation displayed lower biomass yield (Yx/s) and lower specific biomass production rate (qX) when compared with cultures grown at excess iron (Fig. 1A, B). In addition, the cultures grown with iron limitation showed increased acetate production rate (qA) and glucose consumption rate (qS) when compared with cultures grown at excess iron (Fig. 1C, D). Lactate was not detectable during YSI biochemistry analysis of culture medium either with iron limitation or iron excess. The iron limitation also decreased the specific O_2 consumption rate (qO_2) and the CO_2 production rate (qCO_2) in cultures controlled at dO_2 of 6.3 % (Table 1), and the respiratory quotient was practically the same, 1.007 ± 0.018 versus 1.02 ± 0.007 (Table 1). These findings suggest a microaerobic-like response of *E. coli*

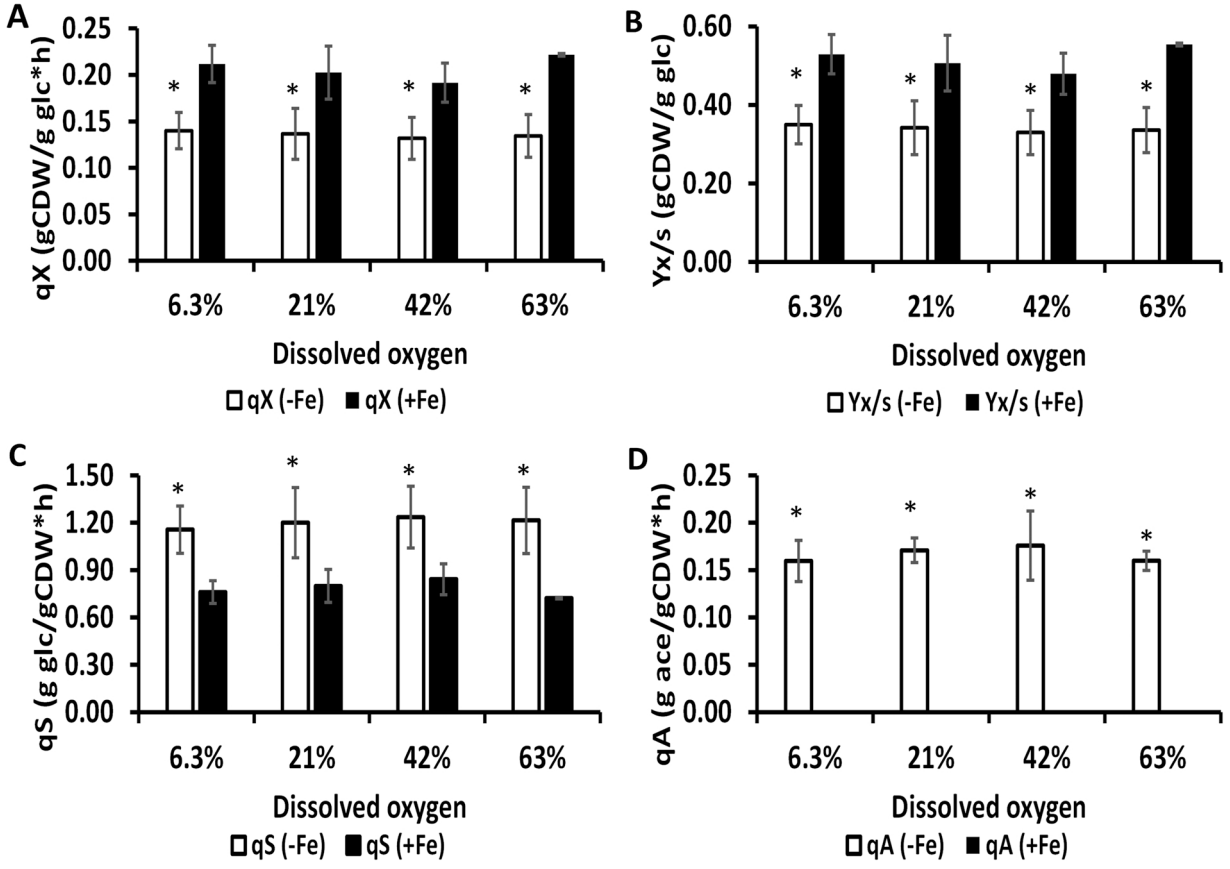

Fig. 1. Growth parameters of steady state cultures (D = 0.4 h^{-1}) with and without iron limitation controlled at different dissolved oxygen concentrations. A. Specific biomass production rate, B. Biomass yield on glucose, C. Specific glucose consumption rate, and D. specific acetate production rate. An asterisk indicates a significant difference between iron limitation and iron excess based on Fisher's LSD test at $p = 0.05$.

Table 1
Respiration parameters of cultures controlled at dO_2 of 6.3 %.

Parameter	Iron limitation	Iron excess
Respiratory quotient	1.007 ± 0.018	1.02 ± 0.007
qO_2 (mmol/gCDW h)	4.740 ± 0.087	9.95 ± 0.085
qCO_2 (mmol/gCDW h)	4.770 ± 0.046	10.16 ± 0.110

growing in iron limitation, independent of the dO_2 concentration in the culture medium.

Effect of dO_2 on accumulation of glutamate, pyruvate and hypoxanthine in E. coli growing at steady state with and without iron limitation

To determine whether the iron limitation affects the pyruvate node and the TCA cycle, pyruvate and glutamate concentrations were determined in the culture medium. The results are summarized in Fig. 2. Iron limitation was associated with higher pyruvate accumulation while the dO_2 concentration had no effect (Fig. 2A). Glutamate concentration was unaffected by either iron limitation or O_2 concentration (Fig. 2B), suggesting that the balanced glucose catabolism was partially reduced, most likely at the pyruvate node, leading to pyruvate and acetate accumulation. Accumulation of hypoxanthine, a degradation product of ATP, in the culture medium is considered a general stress indicator [26], but its concentration was not affected by the iron concentration (Fig. 2C).

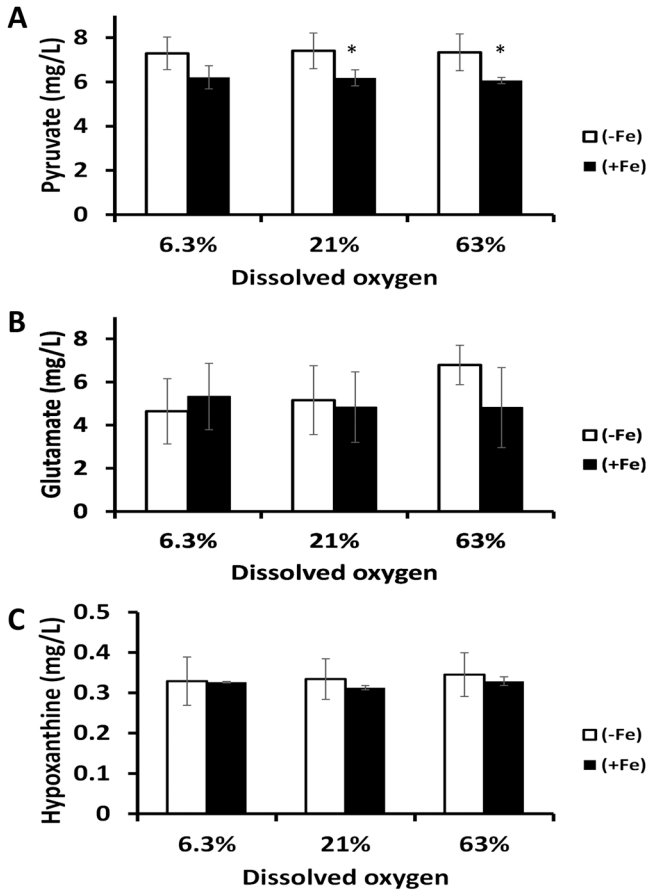

Fig. 2. Extracellular concentrations of glutamate, pyruvate and hypoxanthine in *E. coli* steady state cultures (D = 0.4 h^{-1}) with and without iron limitation at different dissolved oxygen concentrations A. Pyruvate, B. Glutamate, and C. Hypoxanthine. An asterisk indicates a significant difference between iron excess and iron limitation according to Fisher's LSD test at $p = 0.05$.

Effect of dO_2 on siderophore production and peroxidase, superoxide dismutase and catalase activity in E. coli growing at steady state with and without iron limitation

Iron availability affects the activity of several metalloenzymes, such as superoxide dismutase catalase, and peroxidase, and therefore the cells' ability to respond to the harmful effect of the reactive oxygen species formed during aerobic growth. Hence, the presence of 105.6 μM $FeCl_3$ increased the activities of SOD, catalase, and peroxidase (Fig. 3). The activities of peroxidase and SOD increased together with the increased dO_2 concentration (Fig. 3A, B), an indication that elevated O_2 concentrations are associated with increased oxidative stress. Catalase activity was unaffected by the O_2 concentration (Fig. 3C).

When iron is limited, *E. coli* activates enterobactin biosynthesis, the iron acquisition system, that retracts ferric iron into the cells. The amount of siderophore secreted by *E. coli* at iron limitation conditions was measured using the chrome azurol S (CAS) competitive iron-binding capacity assay and the results are shown in Fig. 3D. As expected, iron-limited cultures had higher siderophore production than cultures with excess iron, independent of the dO_2 concentration.

Effect of dO_2 on transcriptomic profile of E. coli growing at steady state with and without iron limitation

Independent of the oxygen availability, iron limitation decreased biomass yield, respiration and antioxidant defenses, while at the same time increasing glucose consumption, pyruvate, and acetate secretion, mimicking a microaerobic conditions response. To understand the bacterial response to iron limitation at the dO_2 concentrations (6.3 %, 21 % and 63 %), a comparative transcriptomic analysis was conducted. Transcriptomic analysis (iron excess over iron limitation) at 6.3 %, 21 % and 63 % dO_2 resulted in 145, 127, and 194 upregulated genes (> 1.5 fold change, $p < 0.05$) and 26, 75, and 154 downregulated genes (< -1.5 fold change, $p < 0.05$) (Supplementary Table 1). Among the DEGs, 31 were upregulated and 16 were downregulated in all dO_2 conditions shown by the Venn diagram in Fig. 4. Functional annotation and over-representation of the upregulated and downregulated genes of GO terms ($p < 0.05$) were performed. The results showed that excess iron increased the expression of genes involved in putrescine (*puuA*, *puuB*, *puuC*, *puuD,* and *puuE*) and L-arginine degradation (*astA*, *astB*, *astC, and astD*) likely to increase nitrogen availability. Iron availability also increased the transcription of genes involved in the detoxification of copper and silver ions as part of the CusCFBA copper/silver efflux system (*cusA*, *cusB*, and *cusC*), and increased the expression of *sodB* and other genes involved in propanoate degradation (*prpB*, *prpC*, *prpD*, and *prpE*). At the same time, excess iron downregulated genes involved in siderophore biosynthesis (*entA*, *entB*, *entC*, *entD*, *entE*, and *entF*), iron (III) transport (*fhuE*, *fepA*, and *fiu*), and protein folding/response to pH (*hdeA*, *hdeB*, and *hdeD*) (Supplementary Table 1).

The functional clustering of genes that were upregulated at 6.3% dO_2 with iron excess revealed the enrichment of genes involved in multihaem cytochrome *c* proteins of the anaerobic electron transport chain formed by hydrogenase and nitrate reductase or DMSO reductase (Table 2). Excess iron at 21 % and 63 % dO_2 was associated with upregulation of genes involved in the respiratory chains formed by hydrogenase 2 and TMAO, nitrate, and fumarate reductases (Table 2), which are normally used in anaerobic conditions. The functional clustering of the 84 genes that were upregulated only at 6.3% dO_2 with iron excess (Supplementary Table 1) revealed the enrichment of genes involved in phenolic compound degradation (*hcaF*, *mhpB*, and *paaZ*) and citrate lyase activation (*citC*, *citE*). The 23 genes that were upregulated at 21 % dO_2 exclusively by excess iron, were not functionally clustered (Supplementary Table 1). There were 108 specific genes that were upregulated by excess iron only at 63 % dO_2 (Supplementary Table 1). The overrepresented functional groups for these specific genes were for bacterial chemotaxis (*aer*, *malE*, *mglB*, *rbsB*, *trg*, and *uspF*), sugar

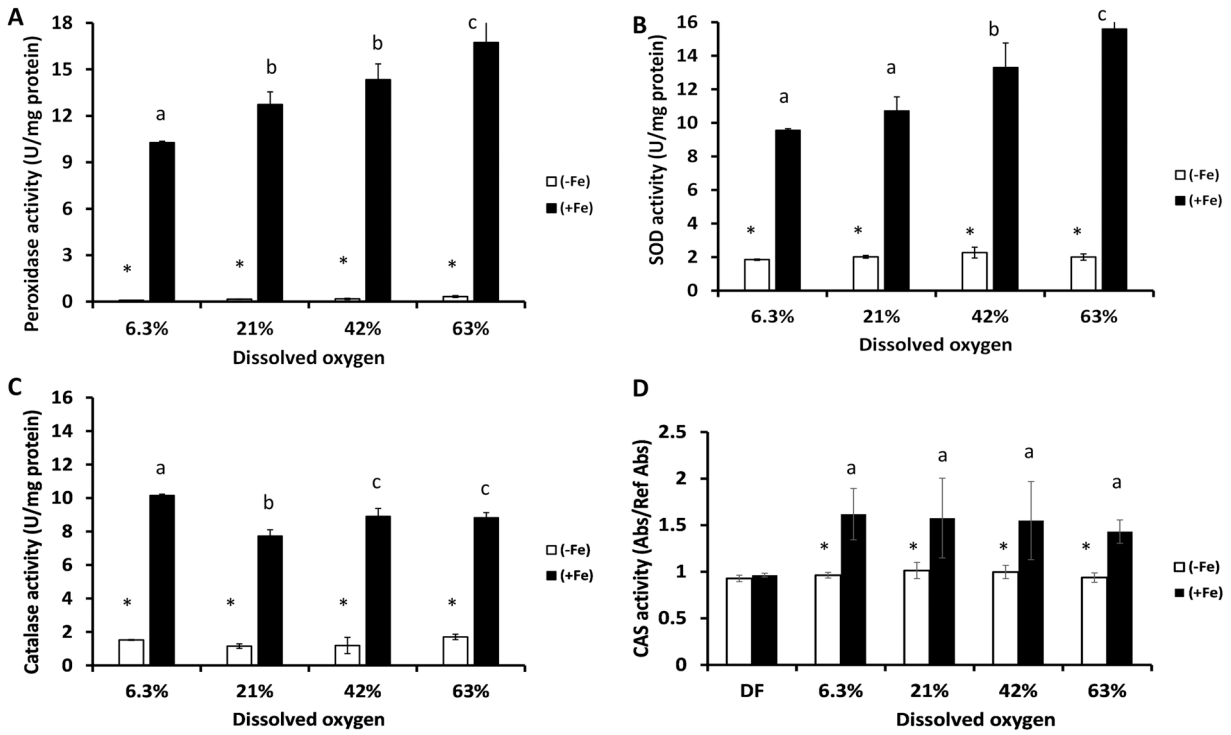

Fig. 3. Activity of peroxidase, superoxide dismutase and catalase with and without iron limitation at steady state conditions at different oxygen concentrations. DF is positive control of sterile medium containing 15 μM deferoxamine (Desferal). Different letters indicate significant differences between different oxygen concentrations in cultures with iron excess according to LSD at $p = 0.05$. An asterisk indicates a significant difference between iron excess and iron limitation based on Fisher's LSD test at $p = 0.05$.

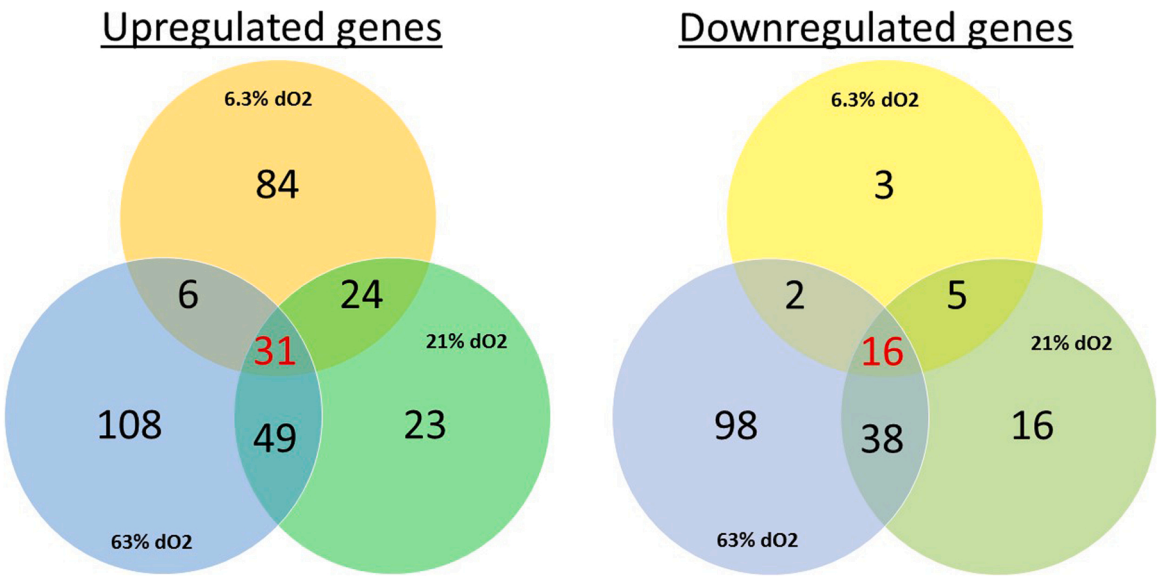

Fig. 4. Venn diagram of transcriptomics data at different dissolved oxygen concentrations. Analysis was performed from data obtained from bacteria grown in minimal medium with and without iron limitation.

transport (*rbsA, malEK, xylF, xylG, mglB, rbsB, chiP, and treB*), and fatty acid degradation (*fadB, fadD, fadE, fadI,* and *fadJ*). Excess iron downregulated three specific genes at 6.3 % dO_2 and 16 at 21 % dO_2 (Fig. 4 and Supplementary Table 1), which were not clustered with a significant *p*-value. For cultures at 63 % dO_2, iron excess downregulated 98 specific genes (Supplementary Table 1 and Fig. 4). These repressed genes were clustered in the amino acid transmembrane transport group (*gadC*, *plaP*, *ydgI*, *yjeM*, and *tyrP*) and the rRNA processing group (*rlmA*, *rlmC*, *rlmF*, *rlmG*, *rsmF*, *rluC*, and *truC*), activity of which is required for translation and cell growth.

The effects of dO_2 upshifts on gene expression were evaluated at steady-state conditions with and without iron limitation (Supplementary Table 2). Increasing dO_2 to 63 % in cultures with iron excess upregulated genes encoding for ribonucleoside-diphosphate reductase (NrdF), dimanganese-tyrosyl radical cofactor maintenance flavodoxin (NrdI), and glutaredoxin-like protein (NrdH), all required for activity of class Ib ribonucleotide reductase, which normally is induced by oxidative stress. Oxygen upshifts also increased the transcription of the ferric

Table 2
Up regulation of dehydrogenases and terminal reductases of the respiratory chains of *E. coli* by iron excess in aerobic conditions (transcriptomic and **proteomic** level). In *italic* are the repressed ones.

dO_2 Conc (%)	Dehydrogenases	Genes/protein	Redox pair	Terminal reductases	Genes	Redox pair
6.3	Hydrogenase 2	*hybAB*	H^+/H_2	Nitrate reductase Z	*narZU*	NO_3^-/NO_2^-
	NADH DH I	**NuoA-L**	NAD^+/NADH	Periplasmic nitrate reductase	*napABCGH*	NO_3^-/NO_2^-
	Pyruvate oxidase	**PoxB**	Acetate + CO_2/pyruvate	Nitrite reductase	*nrfB*	NO_2^-/NH_4^+
	Glucose DHD	**Gcd**	Glucose/gluconate	DMSO reductase	*dmsA*	DMSO/DMS
	-amino acid DH	**DadA**	2-oxoacid + NH_4 +/amino acid			
	NADH DH II	**Ndh**	NAD^+/NADH			
21	Hydrogenase 2	*hybAB*	H^+/H_2	Periplasmic nitrate reductase	*napGH*	NO_3^-/NO_2^-
				DMSO reductase	*dmsAB*	DMSO/DMS
				Fumarate reductase	*frdBCD*	Fumarate/succinate
63	Hydrogenase 2	*hybA*	H^+/H_2	Periplasmic nitrate reductase	*napH*	NO_3^-/NO_2^-
	NADH DH I	**nuoA-L**	NAD^+/NADH	TMAO reductase	*torY*	TMAO/TMA
	Pyruvate oxidase	**PoxB**	Acetate + CO_2/pyruvate	Fumarate reductase	*frdBC*	Fumarate/succinate
	Glucose DHD	**Gcd**	Glucose/gluconate			
	-amino acid DH	**DadA**	2-oxoacid + NH_4 +/amino acid			
	NADH DH II	**Ndh**	NAD^+/NADH			

enterobactin esterase (*fes*) and enterobactin biosynthesis protein (*ybdZ*), both usually activated in response to iron-limiting conditions. Under excess iron conditions, high O_2 led to repression of genes involved in cyanate degradation (*cynS* and *cynT*) and periplasmic diheme cytochrome c550 components of periplasmic nitrate reductase (*napABG*) and hydrogenase 2 (*hybB*) (Supplementary Table 2).

In cultures with iron limitation, elevated O_2 upregulated genes involved in biofilm formation (*dgcJ*, *dgcN*, *pdeF*, *yafQ*, *ycbU*, and *yqcC*), biosynthesis of extracellular polysaccharide (*wcaD* and *wcaL*), detoxification efflux pumps (*emrY* and *mdtL*), and DNA damage response (*emrY*, *gadW*, *hprS*, *hyfF*, *nikE*, *ybfE*, *xseA*, *ybiJ*, and *ycjW*) (Supplementary Table 2). Under these conditions, high O_2 concentrations downregulated genes involved in fatty acid degradation (*fadA*, *fadB*, *fadD*, *fadI*, and *fadJ*), D-mannose degradation (*manY*, *manZ*), D- and L-arabinose degradation (*aldA*, *fucA*, *araA*, *araB*) and translation initiation (*epmA*, *infA*, *rpsT*, *rpsU*, *yafQ*).

Effect of dO_2 on proteomic profile of E. coli growing at steady state with and without iron limitation

Similar to the effect of oxygen on the transcriptomic, the proteomic analysis at 6.3 % dO_2 showed that excess iron decreased the expression of proteins involved in siderophore/enterobactin synthesis (EntA, EntB, EntC, EntE, and EntF) and iron transport (EfeO, FepA, FhuE, Fiu, and FeoB), while it activated the protein expression of propanoate (propionate) degradation (PrpB, PrpC, and PrpD,), the CusCFBA copper/silver efflux system (CusA, CusB, and CusC), and the superoxide dismutase B (SodB) (Supplementary Table 3), showing that expression of these gene products was differentiated at both transcript and protein levels. Excess iron also increased the protein expression of the respiratory chain formed by NADH dehydrogenase I (NuoA, NuoB, NuoC, NuoE, NuoG, and NuoI), and the TCA cycle (AcnA, AcnB, FumA, FumC, SucC, SdhA, and SdhB), whose encoding genes were not affected at the transcriptional level. Conversely, excess iron repressed protein expression of glycolysis (GpmA, PfkA), chorismate biosynthesis (AroA, AroG, AroH) and acetate production (PoxB). A similar protein expression pattern was observed for dO_2 of 63 % in cultures with excess over limitation of iron (Supplementary Table 3).

The effect of oxygen upshift on proteomic profile was also analyzed in cultures with and without iron limitations (Supplementary Table 4). Proteins overexpressed when O_2 increased in cultures with iron availability were cysteine desulfurases (IscU and IscS), ferredoxin (Fdx), transcription factor Iron-sulfur cluster regulator (IscR), iron-sulfur cluster biosynthesis chaperones (HscA, HscB), and the iron-sulfur cluster carrier protein (NfuA), all of which are required for assembly of iron-sulfur clusters. Over oxygenation also increased the expression of proteins involved in oxidative stress (PpiC and FumC), and at the same time repressed the mechanosensitive channel (MscS) and the sensor of cell envelope defects (RcsF) (Supplementary Table 4). At iron-limited conditions, over oxygenation triggered the overexpression of the iron-sulfur cluster regulator (IscR), cysteine desulfurase (IscS), and a chaperone (HscB) involved in the regulation of secondary pathways of iron-sulfur cluster assembly, iron-sulfur proteins and anaerobic respiration enzymes. Under these iron limiting conditions, over oxygenation repressed proteins involved in respiration (NADH dehydrogenase I, NuoF), translation (RplN, YeiP), ferrous iron uptake system (FeoB), and membrane transport/translocation (TatA, GatB, FruB, CusB, MalF).

Estimated flux distributions of E. coli growing at steady state with and without iron limitation at dO_2 of 6.3 %

The aerobic flux distribution maps of *E. coli* growing at steady state with and without iron limitation are shown in Fig. 5. The iron limitation flux map was characterized by high flux through glycolysis (1.6-fold higher than iron excess conditions), high carbon flow in the oxidative pentose phosphate pathway (55 % of glucose uptake versus 36 % for iron excess conditions), and low flow through the TCA cycle (3-fold lower than iron excess conditions). Significant fluxes of fermentation metabolites such as formic acid (3.88 mmol/gCDW/h) and acetic acid (2.47 mmol/gCDW/h) were observed in cultures with iron limitation but not with iron excess (Fig. 5). This waste of carbon is consistent with less efficient use of carbon for biomass production under iron-limiting conditions (Fig. 1A, B). Carbon flow through citrate synthase (GltA) and aconitase (AcnB) in the TCA cycle accounted for 11.6 % of the glucose consumption rate for cultures grown in iron limitation and 53.3 % for cultures grown in iron excess. Respiration and central metabolism of cultures grown at iron excess produced about 5.8 mmol ATP per mmol of glucose consumed while cultures grown at iron restricted produced only 2.9 mmol ATP per mmol of glucose consumed, an indication of a restricted cellular energetics caused by iron limitation. Consequently, the flux through the NADH dehydrogenase I and cytochrome bo_3 ubiquinol oxidase at iron excess were 17 % and 29 % higher than iron limiting conditions (Supplementary Table 5).

Discussion

Independently of the oxygenation level, aerobic *E. coli* cultures under iron limitation conditions exhibited lower cellular energetics and a microaerobic-like response that are associated with both lower biomass production and respiration rate (Fig. 1A, B, and Table 1). The impaired respiration rate could be the result of the reduced iron-sulfur cluster containing proteins of the NADH dehydrogenase I and the TCA cycle, such as NuoB, NuoC, NuoE, NuoF, NuoG, NuoI, AcnA, AcnB, SdhA, SdhB, and FumA, which were suppressed at the iron limiting conditions.

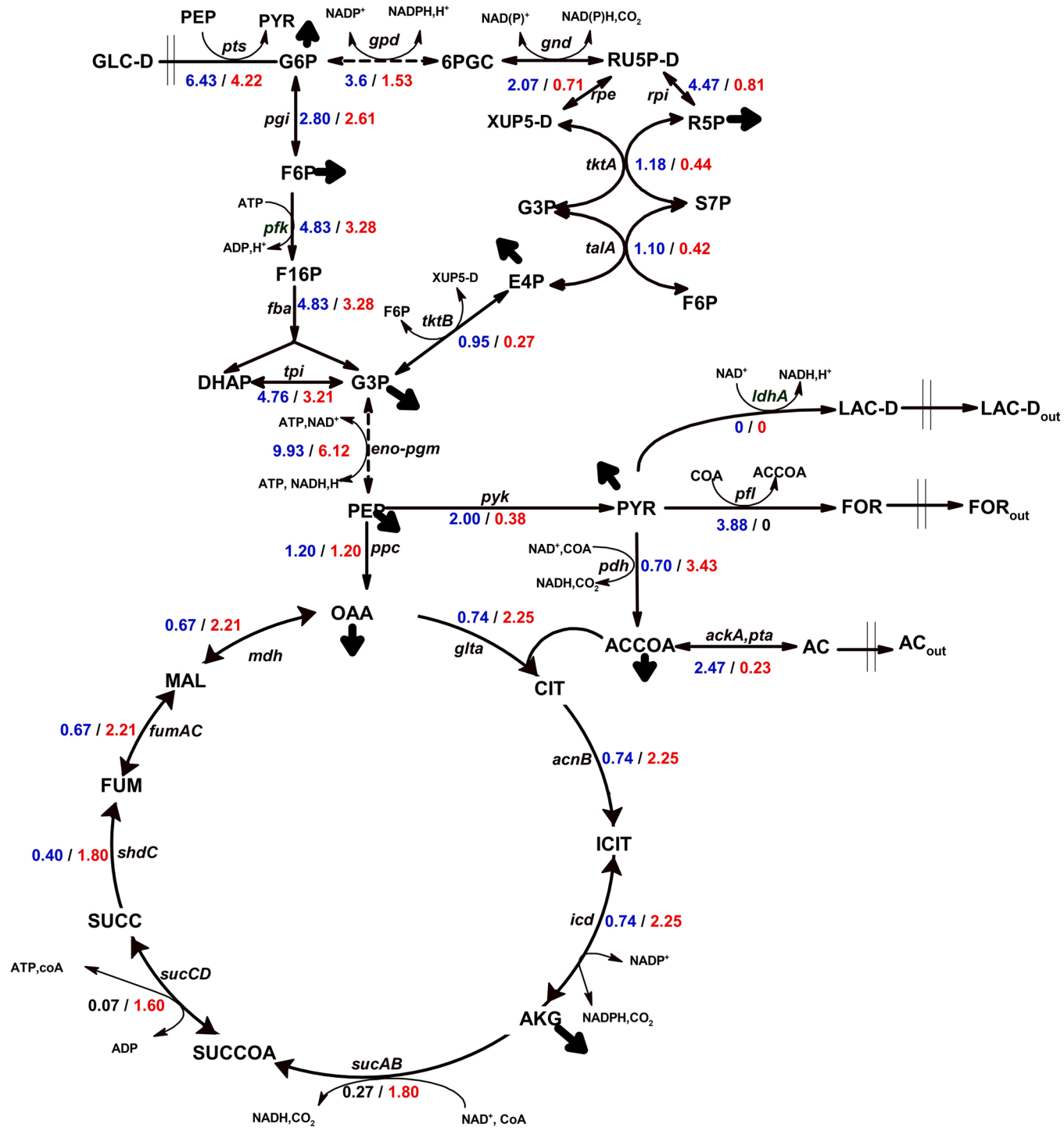

Fig. 5. Comparison of the distribution of the carbon flux in the central metabolism with iron limitation (blue) and iron excess (red). Flux values are reported in mmol $gCDW^{-1}$ h^{-1}.

In addition, iron limiting conditions displayed lower transcription levels of hydrogenase 2 and the terminal reductases of the respiratory chain such as nitrate, nitrite, DMSO, TMAO, and fumarate reductases (Table 2 and Supplementary Table 1), which are also iron-containing proteins. Since cellular iron concentration in *E. coli* increases proportionally with the iron concentration in the growth medium [27,28], it would be expected that cells growing in culture with excess iron have a higher concentration of iron-rich protein complexes, several of which are found in the respiratory chain and the TCA cycle (Table 2 and Supplementary Table 1). Thus, to direct a rational investment of iron and energy to synthesize large complexes of iron-containing enzymes, iron-restricted cells repressed the NADH dehydrogenase I, hydrogenase 2 iron-sulfur protein (*hybA*), periplasmic nitrate reductase cytochrome c_{550} protein (*napB*), periplasmic nitrite reductase penta-heme *c*-type cytochrome (*nrfB*), dimethyl sulfoxide reductase subunit A (*dmsA*), and fumarate reductase iron-sulfur protein (*frdB*) (Table 2).

However, there are inescapable metabolic adjustments associated with this rational iron investment that cells should overcome. The first is the lower cellular energetics (2.9 mmol ATP/mmol glucose at iron limitation versus 5.8 mmol ATP/mmol glucose at iron excess), which are

the result of limited TCA cycle and respiratory chain activities that likely reduced the ATP per glucose yield and hence impaired cell growth. Iron restricted bacteria also displayed lower degradation of L-arginine, putrescine, and cyanate (Supplementary Tables 1 and 3), which probably restricted nitrogen availability to the cells, since all these pathways yield ammonia. Furthermore, iron limitation also decreased propanoate and fatty acid degradation, thus limiting the source of carbon and energy, which explains the lower biomass yield of iron restricted bacteria (Fig. 1B). In response to the low cellular energetics, *E. coli* increased glucose consumption (Fig. 1C) which correlated with increased protein expression of the glycolytic enzymes and higher glycolytic flux (Supplementary Table 3 and Fig. 5). As a result, a bottleneck at the pyruvate node was indicated by the higher accumulation of acetate and pyruvate and flux of formic acid.

It has been proposed [28] that high respiratory activity creates a low local oxygen concentration by generating a rapid flow of electrons from NADH to the inner membrane respiratory complexes, creating a safe environment for oxygen-sensitive enzymes. These respiratory complexes decrease the oxygen concentration to limit its diffusion into the cytosol where oxidative-sensitive processes such as iron-sulfur biosynthesis occur. Consistent with this concept, cultures with excess iron showed higher respiratory activity enabled by the higher iron-rich proteins of the TCA cycle and the respiratory chain. However, this high-yielding ATP metabolic strategy may have increased reactive oxygen species generation [29]. To handle the increased reactive oxygen species, *E. coli* with available iron increased the activities of superoxide, peroxidase, and catalase (Fig. 3), by higher expression of Fe-SOD (SodB) and catalase/hydroperoxidase HPI (KatG) (Supplementary Table 3).

E. coli cultures grown at excess iron upregulated the transcription and translation of the CusCFBA copper/silver efflux system compared with iron restricted cultures. Excess Fe (III) and oxidative stress block the binding of CueR to the *copA* promoter and decrease the expression of the primary copper detoxification system CopA, and at the same time activate the secondary copper detoxification system CusCFBA [30]. In this way, cultures at excess iron, whose respiration and reactive oxygen species production is higher, induce the CusCFBA efflux system to lower intracellular Cu(I) content [31]. It is therefore plausible that during iron excess conditions, *E. coli* activates the CusCFBA copper efflux systems to protect iron-sulfur cluster enzymes from elevated concentrations of cellular copper ions [31]. This hypothesis is supported by the higher flux of Fe^{2+} through the iron-sulfur cluster repair system (FESR) predicted by the metabolic flux analysis (Supplementary Table 5).

The cellular response to over oxygenation was different in excess and in limiting iron conditions. When iron is available, over oxygenation affects pathways of iron-sulfur cluster assembly, iron-sulfur proteins, and anaerobic respiration of enzymes containing iron, possibly by the accumulation of reactive oxygen species [29]. As a result, the expected higher concentrations of the latter activate the transcription of the oxidative stress insensitive *nrdHIEF* operon and the activity of peroxidase and SOD (Fig. 3A, B). *E. coli* also activated the assembly of iron-sulfur clusters by increasing the amount of cysteine desulfurase (IscS), the scaffold protein (IscU), the iron chaperones (HscAB), the ferredoxin (Fdx), and the DNA-binding transcriptional regulator IscR. When iron was scarce, over-oxygenation induced biofilm formation and biosynthesis of extracellular polysaccharides while repressing fatty acid degradation (Supplementary Table 2), likely to reduce oxygen diffusion into the cytoplasm, avoiding the detrimental effects of elevated oxygen concentrations on the labile Fe^{2+} pool [28].

Conclusion

In summary, when iron is available at moderate or at high oxygenation, *E. coli* maintains high cellular energetics (5.8 ATP/mol of glucose) by using pathways requiring iron-rich complex proteins found in the TCA cycle and electron transport chain. Several iron-requiring terminal reductases of the respiratory chain, that were considered to be anaerobic, are used in aerobic conditions with excess iron to keep high respiratory activity. This high energetic state allows *E. coli* to produce more biomass while investing some energy to repair iron-sulfur clusters and deal with oxidative stress. When iron is limited, *E. coli* growing aerobically reduces its respiratory activity and obtains needed energy from fermentative metabolism.

Funding

This research was supported by the Intramural Research Program of the National Institute of Diabetes and Digestive and Kidney Diseases (NIDDK/NIH).

Data availability

Data will be deposited at the NCBI.

Declaration of Competing Interest

The authors declare that they have no known competing financial interests or personal relationships that could have appeared to influence the work reported in this paper.

Data availability

Data will be made available on request.

Acknowledgement

The authors would like to thank Yolanda L. Jones, NIH Library, for editing assistance.

Appendix A. Supporting information

Supplementary data associated with this article can be found in the online version at doi:10.1016/j.nbt.2022.06.004.

References

[1] Beauchene NA, Mettert EL, Moore LJ, Keleş S, Willey ER, Kiley PJ. O_2 availability impacts iron homeostasis in *Escherichia coli*. Proc Natl Acad Sci USA 2017;114(46):12261–6. https://doi.org/10.1073/pnas.1707189114.
[2] Baez A, Shiloach J. Increasing dissolved oxygen disrupts iron homeostasis in production cultures of *Escherichia coli*. Antonie Van Leeuwenhoek 2017;110(1):115–24. https://doi.org/10.1007/s10482-016-0781-7.
[3] Jacques JF, Jang S, Prévost K, Desnoyers G, Desmarais M, Imlay J, et al. RyhB small RNA modulates the free intracellular iron pool and is essential for normal growth during iron limitation in *Escherichia coli*. Mol Microbiol 2006;62(4):1181–90. https://doi.org/10.1111/j.1365-2958.2006.05439.x.
[4] Massé E, Vanderpool CK, Gottesman S. Effect of RyhB small RNA on global iron use in *Escherichia coli*. J Bacteriol 2005;187(20):6962–71. https://doi.org/10.1128/JB.187.20.6962-6971.2005.
[5] Keseler IM, Mackie A, Santos-Zavaleta A, Billington R, Bonavides-Martínez C, Caspi R, et al. The EcoCyc database: reflecting new knowledge about *Escherichia coli* K-12. Nucleic Acids Res 2017;45(D1):D543–50. https://doi.org/10.1093/nar/gkw1003.
[6] Andrews SC, Robinson AK, Rodríguez-Quiñones F. Bacterial iron homeostasis. FEMS Microbiol Rev 2003;27(2–3):215–37. https://doi.org/10.1016/S0168-6445(03)00055-X.
[7] McHugh JP, Rodríguez-Quinoñes F, Abdul-Tehrani H, Svistunenko DA, Poole RK, Cooper CE, et al. Global iron-dependent gene regulation in *Escherichia coli*. A new mechanism for iron homeostasis. J Biol Chem 2003;278(32):29478–86. https://doi.org/10.1074/jbc.M303381200.
[8] Massé E, Gottesman S. A small RNA regulates the expression of genes involved in iron metabolism in *Escherichia coli*. Proc Natl Acad Sci USA 2002;99(7):4620–5. https://doi.org/10.1073/pnas.032066599.
[9] Ihssen J, Egli T. Specific growth rate and not cell density controls the general stress response in *Escherichia coli*. Microbiology 2004;150(Pt 6):1637–48. https://doi.org/10.1099/mic.0.26849-0.
[10] Folsom JP, Parker AE, Carlson RP. Physiological and proteomic analysis of *Escherichia coli* iron-limited chemostat growth. J Bacteriol 2014;196(15):2748–61. https://doi.org/10.1128/JB.01606-14.
[11] Folsom JP, Carlson RP. Physiological, biomass elemental composition and proteomic analyses of *Escherichia coli* ammonium-limited chemostat growth, and

comparison with iron- and glucose-limited chemostat growth. Microbiology 2015; 161(8):1659–70. https://doi.org/10.1099/mic.0.000118.
[12] Bauer S, Shiloach J. Maximal exponential growth rate and yield of *E. coli* obtainable in a bench-scale fermentor. Biotechnol Bioeng 1974;16(7):933–41. https://doi.org/10.1002/bit.260160707.
[13] Himpsl SD, Mobley HLT. Siderophore detection using chrome azurol S and cross-feeding assays. Methods Mol Biol 2019;2021:97–108. https://doi.org/10.1007/978-1-4939-9601-8_10.
[14] Nelson DP, Kiesow LA. Enthalpy of decomposition of hydrogen peroxide by catalase at 25 °C (with molar extinction coefficients of H2O2 solutions in the UV). Anal Biochem 1972;49(2):474–8. https://doi.org/10.1016/0003-2697(72)90451-4.
[15] Brioukhanov AL, Durand MC, Dolla A, Aubert C. Response of *Desulfovibrio vulgaris* Hildenborough to hydrogen peroxide: enzymatic and transcriptional analyses. FEMS Microbiol Lett 2010;310(2):175–81. https://doi.org/10.1111/j.1574-6968.2010.02061.x.
[16] Sharma AK, Leppla SH, Pomerantsev AP, Shiloach J. Effect of over expressing protective antigen on global gene transcription in *Bacillus anthracis* BH500. Sci Rep 2018;8(1):16108. https://doi.org/10.1038/s41598-018-34196-y.
[17] Paley S, Parker K, Spaulding A, Tomb JF, O'Maille P, Karp PD. The Omics Dashboard for interactive exploration of gene-expression data. Nucleic Acids Res 2017;45(21):12113–24. https://doi.org/10.1093/nar/gkx910.
[18] Lin Y, Huo L, Liu Z, Li J, Liu Y, He Q, et al. Sodium laurate, a novel protease- and mass spectrometry-compatible detergent for mass spectrometry-based membrane proteomics. PLoS One 2013;8(3):e59779. https://doi.org/10.1371/journal.pone.0059779.
[19] Hains PG, Robinson PJ. The impact of commonly used alkylating agents on artifactual peptide modification. J Proteome Res 2017;16(9):3443–7. https://doi.org/10.1021/acs.jproteome.7b00022.
[20] Boersema PJ, Raijmakers R, Lemeer S, Mohammed S, Heck AJ. Multiplex peptide stable isotope dimethyl labeling for quantitative proteomics. Nat Protoc 2009;4(4): 484–94. https://doi.org/10.1038/nprot.2009.21.
[21] Baez A, Kumar A, Sharma AK, Anderson ED, Shiloach J. Effect of amino acids on transcription and translation of key genes in *E. coli* K and B grown at a steady state in minimal medium. New Biotechnol 2019;49:120–8. https://doi.org/10.1016/j.nbt.2018.10.004.
[22] Orth JD, Conrad TM, Na J, Lerman JA, Nam H, Feist AM, et al. A comprehensive genome-scale reconstruction of *Escherichia coli* metabolism-2011. Mol Syst Biol 2011;7:535. https://doi.org/10.1038/msb.2011.65.
[23] Edwards JS, Covert M, Palsson B. Metabolic modelling of microbes: the flux-balance approach. Environ Microbiol 2002;4(3):133–40. https://doi.org/10.1046/j.1462-2920.2002.00282.x.
[24] Orth JD, Thiele I, Palsson BØ. What is flux balance analysis? Nat Biotechnol 2010; 28(3):245–8. https://doi.org/10.1038/nbt.1614.
[25] Heirendt L, Arreckx S, Pfau T, Mendoza SN, Richelle A, Heinken A, et al. Creation and analysis of biochemical constraint-based models using the COBRA Toolbox v.3.0. Nat Protoc 2019;14(3):639–702. https://doi.org/10.1038/s41596-018-0098-2.
[26] Li Z, Rinas U. Recombinant protein production-associated metabolic burden reflects anabolic constraints and reveals similarities to a carbon overfeeding response. Biotechnol Bioeng 2021;118(1):94–105. https://doi.org/10.1002/bit.27553.
[27] Hohle TH, O'Brian MR. Metal-specific control of gene expression mediated by *Bradyrhizobium japonicum* Mur and *Escherichia coli* Fur is determined by the cellular context. Mol Microbiol 2016;101(1):152–66. https://doi.org/10.1111/mmi.13381.
[28] Wofford JD, Bolaji N, Dziuba N, Outten FW, Lindahl PA. Evidence that a respiratory shield in *Escherichia coli* protects a low-molecular-mass FeII pool from O2-dependent oxidation. J Biol Chem 2019;294(1):50–62. https://doi.org/10.1074/jbc.RA118.005233.
[29] Baez A, Shiloach J. Effect of elevated oxygen concentration on bacteria, yeasts, and cells propagated for production of biological compounds. Microb Cell Fact 2014; 13:181. https://doi.org/10.1186/s12934-014-0181-5.
[30] Xu Z, Wang P, Wang H, Yu ZH, Au-Yeung HY, Hirayama T, et al. Zinc excess increases cellular demand for iron and decreases tolerance to copper in *Escherichia coli*. J Biol Chem 2019;294(45):16978–91. https://doi.org/10.1074/jbc.RA119.010023.
[31] Macomber L, Imlay JA. The iron-sulfur clusters of dehydratases are primary intracellular targets of copper toxicity. Proc Natl Acad Sci USA 2009;106(20): 8344–9. https://doi.org/10.1073/pnas.0812808106.